Acta Pharmaceutica Sinica B 2022;12(8):3383–3397

Chinese Pharmaceutical Association
Institute of Materia Medica, Chinese Academy of Medical Sciences

Acta Pharmaceutica Sinica B

www.elsevier.com/locate/apsb
www.sciencedirect.com

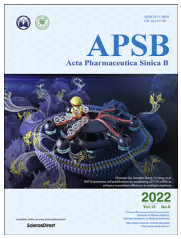

ORIGINAL ARTICLE

Immunogenic hydrogel toolkit disturbing residual tumor "seeds" and pre-metastatic "soil" for inhibition of postoperative tumor recurrence and metastasis

Minglu Zhou, Qingting Zuo, Yuan Huang, Lian Li*

Key Laboratory of Drug-Targeting and Drug Delivery System of the Education Ministry and Sichuan Province, Sichuan Engineering Laboratory for Plant-Sourced Drug and Sichuan Research Center for Drug Precision Industrial Technology, West China School of Pharmacy, Sichuan University, Chengdu 610041, China

Received 11 November 2021; received in revised form 18 January 2022; accepted 6 February 2022

KEY WORDS

Hydrogel;
Postoperative treatment;
Tumor recurrence;
Pre-metastatic niche;
CXCR4 inhibition;
Immunotherapy;
Local therapy;
Immunogenic cell death

Abstract Tumor recurrence and metastasis is the leading cause of mortality for postoperative breast cancer patients. However, chemotherapy intervention after surgery is often unsatisfactory, because residual microtumors are difficult to target and require frequent administration. Here, an all-in-one and once-for-all drug depot based on *in situ*-formed hydrogel was applied to fit the irregular surgical trauma, and enable direct contact with residual tumors and sustained drug release. Our immunological analysis after resection of orthotopic breast tumor revealed that postsurgical activation of CXCR4–CXCL12 signal exacerbated the immunosuppression and correlated with adaptive upregulation of PD-L1 in recurrent tumors. Thus, a multifunctional hydrogel toolkit was developed integrating strategies of CXCR4 inhibition, immunogenicity activation and PD-L1 blockade. Our results showed that the hydrogel toolkit not only exerted local effect on inhibiting residual tumor cell "seeds" but also resulted in abscopal effect on disturbing pre-metastatic "soil". Furthermore, vaccine-like effect and durable antitumor memory were generated, which resisted a secondary tumor rechallenge in 100% cured mice. Strikingly, one single dose of such modality was able to eradicate recurrent tumors, completely prevent pulmonary metastasis and minimize off-target toxicity, thus providing an effective option for postoperative intervention.

*Corresponding author. Tel./fax: +86 28 85501617.
E-mail address: liliantripple@163.com (Lian Li).

Peer review under responsibility of Chinese Pharmaceutical Association and Institute of Materia Medica, Chinese Academy of Medical Sciences.

https://doi.org/10.1016/j.apsb.2022.02.017

1. Introduction

Surgery is currently the main modality to eliminate breast cancer in clinical practice, but recurrence and metastasis after surgery are still common[1,2]. Due to incomplete resection, residual tumors in surgical incision are tiny, scattered, and difficult to be targeted by postoperative intervention of conventional chemotherapy or radiotherapy[3,4]. Immunotherapy that harnesses the host's own immunity to recognize and attack the residual tumors is a promising option[5–7], but still plagued with postsurgical challenges. In one aspect, surgery inevitably stimulates various events (*e.g.*, inflammation) and consolidates immunosuppressive state in surgical trauma, rendering residual tumor "seeds" irresponsive to immunotherapy[8,9]. In another aspect, although surgery removes most of solid tissue of primary tumor, pre-metastatic niche (PMN) in distant organs has already been established, providing a fertilized "soil" permissive for cancer metastasis[10,11]. Therefore, there is an urgent need to devise on-demand strategy for postoperative immunotherapy capable of both (1) reversal of immunosuppressive microenvironment to inhibit residual tumor seeds and (2) blockade of influence from pre-existing PMN soil to minimize the risk of distant metastasis.

Our recent research has reported an *N*-(2-hydroxypropyl) methacrylamide (HPMA) polymer-based strategy that potentiates anti-programmed cell death 1 ligand 1 (PD-L1) therapy in metastatic breast cancer by increasing the immunogenicity of orthotopic tumor and reducing the effect of distant PMN[12]. This strategy involves (1) HPMA copolymer-doxorubicin conjugates (P-DOX), and (2) HPMA copolymer-CXC chemokine receptor 4 (CXCR4) antagonist conjugates [P-$(LV)_6$)]. After intravenous injection, P-DOX passively accumulates in primary tumor, induces immunogenic cell death (ICD), and eventually recruits anti-tumor T cells. Meanwhile, P-$(LV)_6$ actively targets and multivalently crosslinks CXCR4 receptors overexpressed on cancer cells resulting in considerable CXCR4 depletion, which reduces tumor trafficking of immunosuppressive cells that impairs T cells and blocks interaction with pro-metastatic CXCL12 chemokine that is secreted from pulmonary PMN. Such approach with simultaneous activation of anti-tumor immunity and reversal of immunosuppressive tumors and metastasis-prompting PMN fits above criteria for postoperative immunotherapy, but still faces several issues. Firstly, the triple combination of two polymer conjugates and one anti-PD-L1 antibody requires repeated administration *via* systemic injection, which greatly decreases patient compliance; secondly, residual microtumors hiding sporadically at the edge of a resection may not be reached by adequate amount of intravenously administered drug formulations to achieve desired therapeutic effect; thirdly, it remains unknown that how such combination strategy adapts to the changes in the microenvironment after tumor surgery.

To address aforementioned concerns, we herein developed a once-for-all and all-in-one hydrogel toolkit containing P-DOX, P-$(LV)_6$ and anti-PD-L1 antibody (Scheme 1). This hydrogel could be *in situ* formed immediately after syringeable hydrogel precursor polyvinyl alcohol (PVA) and reactive oxygen (ROS) liable crosslinker are concurrently and separately injected to fit the irregular surgical incision[13]. In response to elevated level of ROS in surgical trauma, the hydrogel toolkit would gradually degrade and enable sustained *in situ* release of the polymer-drug conjugates (PDCs) and monoclonal antibody (mAb). As the major advance, direct injection of the drug depot into surgical resection can avoid blood circulation of drugs and increase their contact with residual tumors at operation site[14,15]. Our finding revealed that CXCR4−CXCL12 axis were activated in both postsurgical microenvironment and pulmonary PMN, which substantially contributed to immunosuppression and metastasis. Notably, we also showed that the hydrogel toolkit, with the capabilities of ICD induction, CXCR4 inhibition, and PD-L1 blockade, directly turned the residual tumor seeds into *in situ* vaccine and remotely disturbed the formation of PMN, allowing for a durable immune-memory effect against post-surgery tumor recurrence and metastasis.

2. Materials and methods

2.1. Materials

4-(Bromomethyl) phenylboronic acid, *N*,*N*,*N*′,*N*′-tetramethyl-1,3-propanediamine and poly(vinyl alcohol) (PVA, ∼75 kDa, 99% hydrolyzed) were purchased from Aladdin Biotech Co., Ltd. (Shanghai, China). Anti-CRT antibody, anti-PI3K antibody and Alexa Fluor 647-conjugated secondary antibody were purchased from Abcam (Cambridge, UK). Anti-CD3-FITC, anti-CD4-PerCP, anti-CD8-APC, anti-IFN-γ-PE, anti-CD45-PerCP/Cy5.5, anti-PD-L1-PE and anti-CXCR4-APC antibodies were purchased from Biolegend (San Diego, CA, USA). Anti-CD11b-PE and anti-Gr1-FITC antibodies were purchased from eBioscience (Carlsbad, CA, USA). Anti-CD16/32, anti-Foxp3-PE antibodies, Transcription Factor Buffer Set and Matrigel were purchased from BD Biosciences (Bedford, UK). Anti-MMP-9, anti-LOX, anti-IL-10, anti-S100A8 and anti-TGF-β antibodies were purchased from Servicebio Technology (Wuhan, China). 4′,6-Diamidino-2-phenylindole (DAPI) was purchased from Solarbio Science & Technology Co., Ltd. (Beijing, China). Anti-PD-L1 antibody (mAb) was purchased from BioXcell (Clone: 10F.9G2, West Lebanon, NH, USA). Polymer-drug conjugates (PDCs) including multivalent *N*-(2-hydroxypropyl) methacrylamide (HPMA) copolymer-peptide antagonist to CXCR4 (P-$(LV)_6$) and HPMA copolymer-doxorubicin conjugates (P-DOX) were synthesized according to our previous reports[12] and the details were shown in the Supporting information. ROS-unresponsive hydrogel was prepared by crosslinking poly(vinyl alcohol) methacrylate (*m*-PVA) in the presence of photoinitiator (Irgacure 2959) under ultraviolet (UV) light[16,17], the details were shown in the Supporting information. All other reagents were of analytical grade.

2.2. Synthesis of TSPBA

4-(Bromomethyl) phenylboronic acid (1 g, 4.6 mmol/L) and *N*,*N*,*N*′,*N*′-tetramethyl-1,3-propanediamine (0.2 g, 1.5 mmol/L) were added in dimethylformamide (DMF, 20 mL). After stirring at 60 °C for 24 h, the solution was poured into tetrahydrofuran (THF). The precipitation was collected by centrifugation (5000 rpm, 10 min, KDC-140HR, Anhui USTC Zonkia Scientific Instruments Co., Ltd., China). After drying under vacuum, N^1-(4-boronobenzyl)-N^3-(4-boronophenyl)-N^1,N^1,N^3,N^3-tetramethylpropane-1,3-diaminium (TSPBA) was obtained with a yield of 79.81% (0.68 g) and characterized by ^{1}H NMR[18].

2.3. Formation of hydrogel toolkit

PVA (0.5 g) was mixed with deionized water (10 mL). After stirring at 90 °C for 3 h, a clear PVA solution (5%, *w*/*w*) was acquired. Also,

TSPBA (0.5 g) was dissolved in deionized water (10 mL) to obtain the TSPBA solution (5%, *w*/*w*). Blank hydrogel was immediately formed when the PVA solution (100 μL) and the TSPBA solution (100 μL) were mixed together. For the preparation of drug-loaded hydrogel toolkit, PDCs was dissolved in the PVA solution, and mAb was added to the TSPBA solution. Hydrogel toolkit [P-DOX: 3.80 mg/mL, P-$(LV)_6$: 0.79 mg/mL, mAb: 0.25 mg/mL, 200 μL] was immediately formed when the TSPBA solution containing mAb (100 μL) was added into the PVA solution containing PDCs (100 μL). These hydrogels were used for *in vitro* experiments. For *in vivo* administration, the PVA solution (containing or not containing PDCs at therapeutically relevant doses: DOX, 5 mg/kg; LV, 1 mg/kg; 100 μL) and the TSPBA solution (containing or not containing mAb at therapeutically relevant doses: mAb, 2.5 mg/kg; 100 μL) were loaded into syringes and injected directly into the tumor-resection cavity to form a gel *in situ*.

2.4. *Characterization of hydrogel toolkit*

The dynamic rheological behavior of hydrogel precursor (PVA solution), blank hydrogel and hydrogel toolkit at 25 °C were measured using a TA Instruments AR 2000 rheometer with 25-mm parallel plates (Milford, MA, USA). Storage modulus (G′) and loss modulus were recorded with shear strain of 1% and oscillation frequency from 0.1 to 10 rad/s. The morphology of hydrogel toolkit was characterized by scanning electron microscope (SEM, SU3500/Aztec X-Max20, Oxford, UK). Fluorescence imaging of hydrogel toolkit was analyzed using a confocal microscope (CLSM, Zeiss LSM 510 DUE, Oberkochen, Germany).

2.5. *The ROS-responsive degradation of hydrogel toolkit*

For *in vitro* investigation, hydrogel toolkit (200 μL) was immersed in 8 mL phosphate buffer solution (PBS, pH 7.4) or PBS buffer containing 1 mmol/L H_2O_2 (pH 7.4) at 37 °C. At predetermined time point, the morphology of samples was observed by photos. The drug release behavior was also detected in the PBS buffer with or without 1 mmol/L H_2O_2. P-DOX, fluorescein 5(6)-isothiocyanate FITC labeled P-$(LV)_6$ or cyanine 5 (Cy5) labeled mAb were loaded in the hydrogels for detection. At predetermined time point, 100 μL of solution was collected and replaced with corresponding fresh PBS. The released of P-DOX, P-$(LV)_6$ and mAb were determined by measuring the fluorescence intensity of DOX, FITC and Cy5 *via* Varioskan Flash (ThermoFisher Scientific, Waltham,

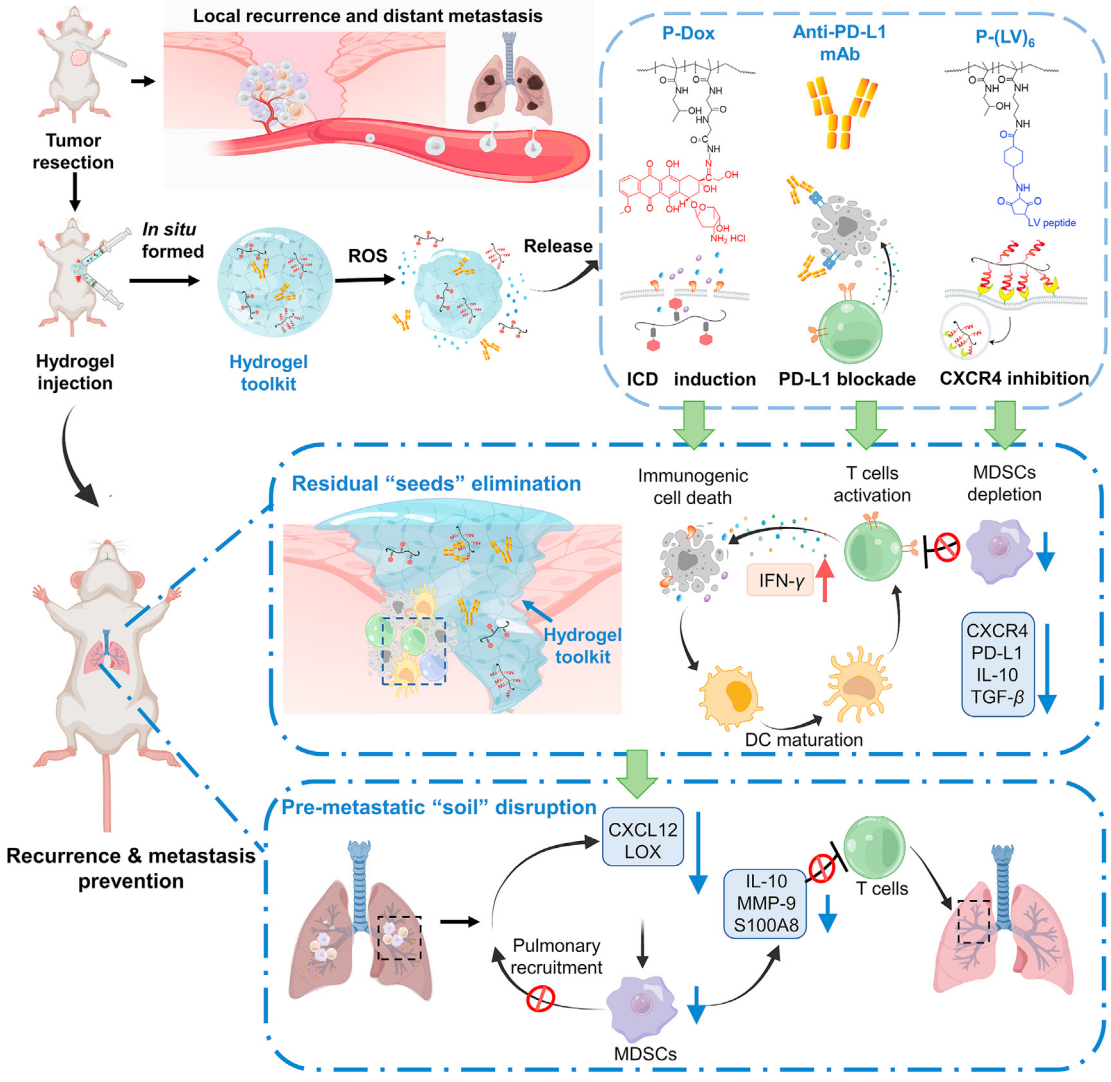

Scheme 1 Schematic illustration of *in situ* formed hydrogel toolkit to disturb residual tumor "seeds" and pre-metastatic "soil" for prevention of postoperative tumor recurrence and metastasis.

MA,USA). Each assay was repeated in triplicate. For *in vivo* evaluation, the H_2O_2 level in the surgical sites was first measured *via* a hydrogen peroxide assay kit (Jiancheng Bioengineering Institute, Nanjing, China). Hydrogel toolkit (200 μL) was injected into the tumor-resection cavity. At predetermined time points, *in situ* hydrogels were collected, photographed and weighted.

2.6. Cell lines and animals

Murine breast cancer cell line (4T1) was purchased from Shanghai Institute of Biochemistry and Cell Biology (SIBCB, China). Luciferase-expressing 4T1 (4T1-Luc) cells was purchased from Icell Bioscience Inc. (Shanghai, China). All cells were cultured in RPMI 1640 medium supplemented with 10% fetal bovine serum and 1% antibiotics (penicillin and streptomycin) at 37 °C under the air atmosphere of 5% CO_2. All experiments were performed on cells in the logarithmic growth phase. Female BALB/c mice (6−8 weeks, 18−22 g, SPF) were purchased from Dashuo Experimental Animal Company (Chengdu, China). All animal experiments were executed according to the protocols approved by Sichuan University Animal Care and Use Committee.

2.7. Postsurgical alterations in tumor microenvironment and pre-metastatic niche

A postoperative breast cancer model was established by resecting around 95% of the tumors with a size of ∼200 mm^3 on Day 12 after 1×10^6 4T1 cells were injected into the third mammary fat pad of female BALB/c mice[9,19]. The resected tumors were collected as preoperative samples. When the volume of residual tumors regrew to nearly 200 mm^3 on Day 19, tumors and lungs were collected as postoperative samples. Meanwhile, a preoperative breast cancer model was established with the same tumor inoculation process but without surgical resection. On Day 12 after tumor inoculation (tumor volume: ∼200 mm^3), lungs were excised as preoperative samples. All samples were homogenized, filtered through 70 μm nylon mesh filters. The red blood cells were lysed using ACK lysing buffer (4 °C, 10 min). To analyze the alternations in tumor microenvironment, the obtained cell suspensions from samples of tumors were blocked with anti-CD16/32 antibody and then stained with indicated antibodies (4 °C, 1 h) for flow cytometry detection: $CD3^+CD8^+$ T cells ($CD3^+CD4^-CD8^+$), myeloid-derived suppressor cells (MDSCs, $CD11b^+Gr1^+$), regulatory T cells (Tregs, $CD3^+CD4^+Foxp3^+$), $CXCR4^+$ cancer cells ($CD45^-CXCR4^+$) and $PD\text{-}L1^+$ cancer cells ($CD45^-PD\text{-}L1^+$) according to the manufacturer's instructions. Tumors were also collected, fixed with 4% paraformaldehyde and cut into thin section (10 μm) to stain with anti-TGF-β antibody. To analyze the alternations in pre-metastatic niche, the obtained cell suspensions from samples of lungs were blocked with anti-CD16/32 antibody and then stained with anti-CD11b-PE to detect $CD11b^+$ bone marrow-derived cells (BMDCs) by flow cytometry. Lungs were also collected and stained with anti-MMP-9 antibody, anti-IL-10 antibody or anti-S100A8 antibody for CLSM detection.

2.8. In vivo anti-recurrence and anti-metastasis effect

To validate anti-recurrence and anti-metastasis effect of hydrogel toolkit, a postoperative breast cancer model was established. 4T1 (1×10^6) cells were injected into the third mammary fat pad of female BALB/c mice (6−8 weeks) and 95% 4T1 tumor (∼200 mm^3) was resected 12 days later. Mice were then randomly divided into 5 groups immediately. Following surgery, different formulations were injected into the surgical bed, including blank hydrogel, mAb@hydrogel, PDCs@hydrogel and hydrogel toolkit (DOX: 5 mg/kg, LV: 1 mg/kg, mAb: 2.5 mg/kg). The recurrent tumor volume and body weight of mice were monitored every two days during the 2-week postoperative period. At the endpoint, tumors were collected to photograph and weight. Meanwhile, metastatic nodules in excised lungs were counted and stained with hematoxylin and eosin (H&E) to determine the degree of metastasis. In addition, the other major organs were collected for H&E staining. Moreover, the long-term outcomes were further evaluated. The postoperative mice model was built and treated as mentioned above. The tumor recurrence and survival of mice were recorded after the tumor resection.

2.9. Immune status investigation

The postoperative mice model was established and treated as indicated above. On Day 14 post tumor resection, recurrent tumors were harvested and homogenized in cold PBS. The obtained cell suspensions were filtered through 70 μm nylon mesh filters and incubated with ACK lysing buffer (4 °C, 10 min) to lysis red blood cells. Afterwards, the remaining cells were collected by centrifugation at 4 °C for 3 min (3000 rpm, KDC-140HR). To investigate the CXCR4 and PD-L1 expression in recurrent tumor, cells were stained with anti-CD45-PerCP/Cy5.5 and anti-CXCR4-APC antibodies (1:200 dilution, 4 °C, 1 h) or anti-CD45-PerCP/Cy5.5 and anti-CXCR4-APC antibodies (1:200 dilution, 4 °C, 1 h) for flow cytometry analysis. To evaluate ICD induction, cells were stained with anti-CD45-PerCP/Cy5.5 and anti-CRT antibodies (1:200 dilution, 4 °C, 1 h). Then, cells were washed and stained with Alexa Fluor 647-conjugated secondary antibody (1:500 dilution, 4 °C, 1 h) for flow cytometry analysis. Meanwhile, CXCR4, PD-L1 and CRT expression were also analyzed by CLSM (Zeiss). Moreover, immune cells in tumor microenvironment were evaluated. To block nonspecific interaction with Fc receptors, cells were first incubated with anti-CD16/32 antibody (4 °C, 30 min) and then stained with indicated antibodies (4 °C, 1h) for flow cytometry detection: $CD3^+CD8^+$ T cells ($CD3^+CD4^-CD8^+$), MDSCs ($CD11b^+Gr1^+$), Tregs ($CD3^+CD4^+Foxp3^+$) according to the manufacturer's protocol. To detect cytokines level, tumors were collected, fixed with 4% paraformaldehyde for 24h and cut into thin section (10 μm) for immunofluorescence staining. The IFN-γ, IL-10 and TGF-β expression were analyzed by CLSM.

2.10. Pre-metastatic niche (PMN) prevention

Since orthotopic 4T1 tumors tend to spontaneously develop lung metastasis, lungs of mice from above immunology survey were collected. Cell suspension was prepared as described above. Afterwards, cells were stained with anti-CD11b-PE (1:300 dilution) to detect the pulmonary recruitment of MDSCs, the key contributor of PMN formation. The other immune cells including $CD3^+CD8^+$ T cells and Tregs were also stained and detected by flow cytometry according to the standard protocols. Meanwhile, representative factors that facilitate the development of PMN, including LOX, MMP-9, IL-10, S100A8, were analyzed by immunofluorescence staining. Lungs were fixed with 4% paraformaldehyde for 24 h and cut into thin slice (10 μm) to stain with anti-MMP-9 antibody, anti-IL-10 antibody or anti-S100A8 antibody and then detected by CLSM. Moreover, the serum levels of TGF-β and LOX, and pulmonary accumulation of CXCL12 were

measured by Elisa kit (SenBeiJia Biological Technology Co., Ltd., Nanjing, China) according to the manufacturer's instructions.

2.11. Long-term immune-memory effect

The postoperative mice model was established and treated with hydrogel toolkit as indicated above with tumor inoculation (s.c.) on Day 0, surgical resection and hydrogel injection on Day 12. Tumor free mice survived from hydrogel toolkit treatment were intravenously injected with 4×10^5 luciferase-expressing 4T1 (4T1-Luc) cells on Day 72. Naïve mice and 4T1 tumor-bearing mice with subsequent tumor resection were also intravenously injected with 4T1-Luc cells to function as controls. *In vivo* bioluminescence in mice was then imaged every week by an IVIS Spectrum Imaging (IVIS Lumina Series III, PerkinElmer, USA). Before imaging, mice were intraperitoneally injected with D-luciferin potassium salt (15 mg/mL, 200 μL). In addition, effector memory T cells ($CD8^+CD62L^-CD44^+$) were analyzed. Spleens were collected and prepared into single cell suspension as described above. Cells were stained with anti-CD8-APC, anti-CD62L-PerCP-Cy5.5, and anti-CD44-PE antibodies (1:200 dilution, 4 °C, 1 h) for flow cytometry detection.

2.12. Pharmacokinetics and biodistribution in vivo

Postoperative breast cancer models were established as described in Section 2.7. Following surgery, hydrogels loaded with Cy5-labled PDCs or mAb (Cy5-P-$(LV)_6$@hydrogel, Cy5-P-Dox@hydrogel, or Cy5-mAb @hydrogel) were locally injected into surgical bed at equivalence of 5 nmol Cy5. By comparison, mice were also intravenously injected with Cy5-P-$(LV)_6$, Cy5-P-Dox or Cy5-mAb (5 nmol Cy5 equivalence). For pharmacokinetic analysis, blood samples (50 μL) were taken from the orbital at predetermined time points, and the fluorescence intensity of each sample was measured using the Varioskan Flash (excitation at 620 nm and emission at 670 nm, ThermoFisher Scientific). For biodistribution analysis, real-time images of anesthetized mice were captured using the IVIS optical imaging system (PerkinElmer), and excised organs at endpoint (12 days post injection) were imaged using the *in vivo* imaging system.

2.13. Statistical analysis

Results were presented as mean ± standard deviation (SD). Statistical analysis was calculated by one-way ANOVA analysis among multiple groups followed by Tukey's multiple comparison or unpaired Student's *t*-test (Graphpad 7.0 and SPSS 22.0 software).

3. Results and discussion

3.1. Postsurgical upregulation of CXCR4–CXCL12 axis correlates with immunosuppression

Surgery can cause pathophysiology stress that affects local and systemic immunity[20]. Since the postoperative intervention of our proposed hydrogel toolkit contains CXCR4-depleting/ICD-inducing PDCs and PD-L1-blocking mAb, we first investigated the postsurgical alterations in relevant immune parameters. A postoperative breast cancer model was established by resecting approximately 95% of the orthotopic tumors (around 200 mm^3) growing in the mammary fat pad of female BALB/c mice[9,19]. When the volume of residual tumors regrew to nearly 200 mm^3, recurrent tumors were resected, analyzed, and compared with presurgical tumors (primarily resected tumors). Our results showed considerable increase in the frequency of tumoral $CXCR4^+$ cells after surgery (Fig. 1A–D), which negatively correlated with the tumor infiltration of $CD8^+$ T immune cells (Fig. 1A) and positively correlated with the abundance of immunosuppressive cells including regulatory T cells (Tregs, Fig. 1B), myeloid-derived suppressor cells (MDSCs, Fig. 1C), and PD-$L1^+$ cancer cells (Fig. 1D). In consistence, enhanced immunosuppression in recurrent tumors has been recognized by other studies[8,21], and we further provided evidence that postsurgical upregulation of CXCR4 may facilitate the evasion of immune surveillance against tumor recurrence.

Ahead of cancer metastasis, primary tumors release lysyl oxidase (LOX) that eventually accumulates at pre-metastatic sites to recruit $CD11b^+$ bone marrow-derived cells (BMDCs)[22]. Thereafter, $CD11b^+$ BMDCs produce various factors (*e.g.*, IL-10, S100A8, MMP-9) to create PMN, a suitable microenvironment for subsequent colonization of disseminated cancer cells[23,24]. Of note, although early metastasis in lung was not detected by the time when the aforementioned presurgical and postsurgical models were analyzed (Fig. 1E), pulmonary accumulation of LOX (Fig. 1F), $CD11b^+$ BMDCs (Fig. 1G), and metastasis-promoting factors of IL-10, S100A8, and MMP-9 (Fig. 1H) were substantially enriched in both models as compared with tumor-free model, demonstrating the formation of distant PMN before surgery. These results suggested that surgery may remove majority of primary tumor, but could not abrogate the impact from PMN which posed a high risk of metastasis.

On the context of spontaneous metastasis, breast cancer preferentially metastasizes to lung which secrets high level of CXCL12 that acts as a chemoattractant that drives $CXCR4^+$ tumor cells towards secondary metastatic sites[25]. Notably, pulmonary CXCL12 secretion in presurgical and postsurgical tumor models increased markedly as compared with tumor-free model, and had positive correlation with increased abundance of recruited MDSCs in lung (Fig. 1I), suggesting the effect of CXCR4–CXCL12 axis persisted even after the tumor resection to facilitate metastasis and immunosuppression. Together, above findings highlighted the great necessity of combining the strategies of CXCR4 depletion, immune activation, and PD-L1 inhibition for postsurgical intervention.

3.2. Preparation and characterization of hydrogel toolkit

Here, local scaffold implantation has been employed for *in situ* release of therapeutic PDCs and mAb at the site of postsurgical tumor (Fig. 2A). First, the PDC of P-$(LV)_6$ capable of multivalently crosslinking/depleting CXCR4 and the PDC of P-DOX capable of sustainably releasing ICD inducer were synthesized according to previous report[12]. The synthetic routes of PDCs with well-defined structures and their characterizations were provided in Supporting Information Fig. S1. Then, ROS-responsive crosslinker N^1-(4-boronobenzyl)-N^3-(4-boronophenyl)-N^1,N^1,N^3,N^3-tetramethylpropane-1,3-diaminium (TSPBA), was synthesized *via* quaternization reaction between N^1,N^1,N^3,N^3-tetramethylpropane-1,3-diamine and 4-(bromomethyl) phenylboronic acid[18]. Mass spectrometry (Thermo Scientific TSQ Quantum Ultra, Carlsbad, CA, USA) was used to validate the synthesis of TSPBA. As shown in Supporting Information Fig. S2, the major peak at *m/z* 200.12 could be assigned to the molecular ion peak ($C_{21}H_{34}B_2N_2O_4^{2+}$,

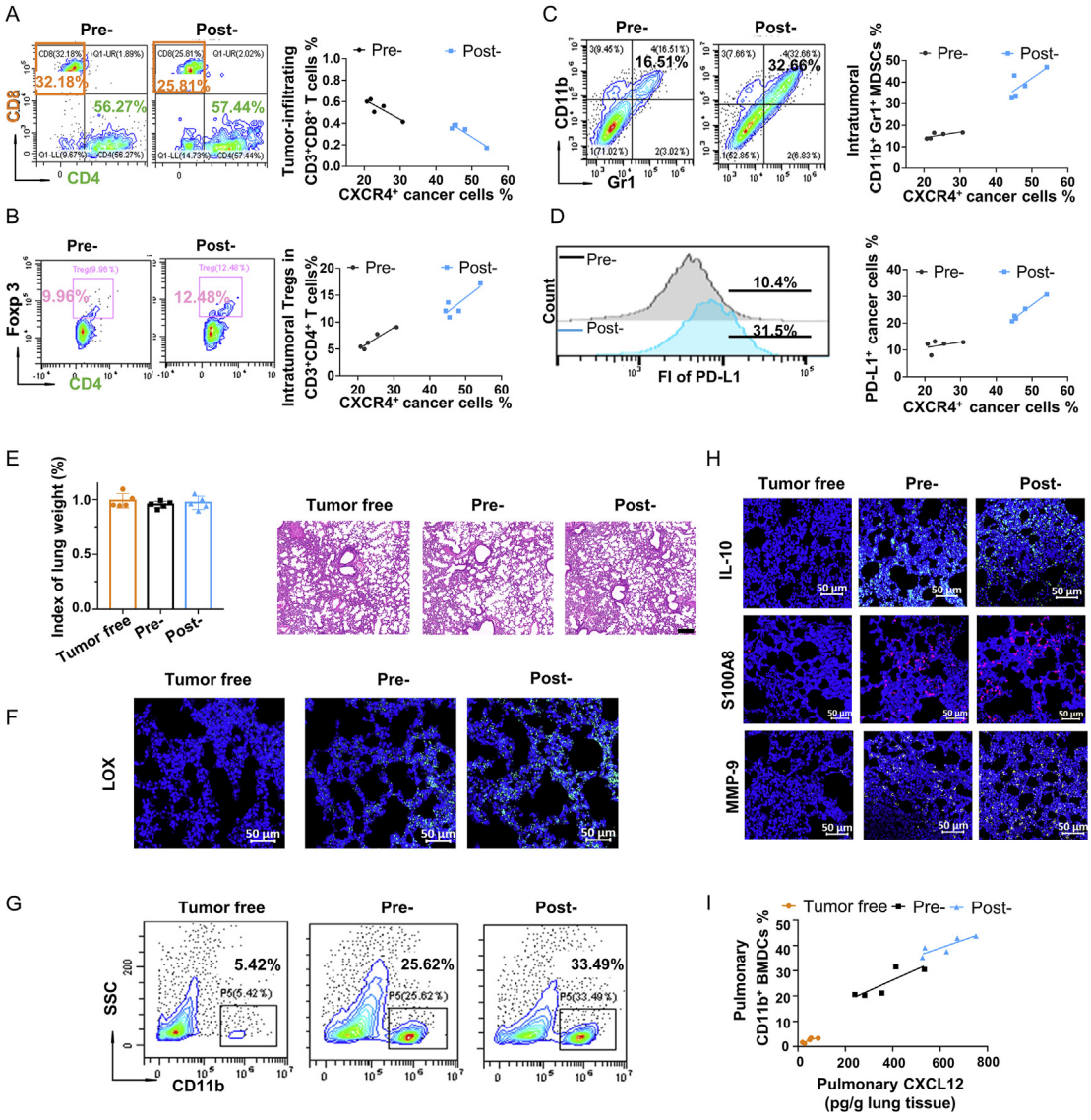

Figure 1 (A) The variations of tumor infiltrating $CD3^+CD8^+$T cells, (B) intratumoral Tregs ($CD3^+CD4^+Foxp3^+$), (C) intratumoral MDSCs ($CD11b^+Gr1^+$) and (D) PD-L1 expression on tumor cells *vs.* CXCR4 expression level in pre-surgical (pre-) or post-surgical (post-) tumors of 4T1-tumor bearing mice ($n = 5$). (E) Lung weight and H&E staining of lung lobe sections. Data are presented as mean ± SD ($n = 3$, scale bar = 100 μm). (F) LOX accumulation (scale bar = 50 μm) (G) pulmonary $CD11b^+$ BMDCs, and (H) IL-10, S100A8 and MMP-9 expression (scale bar = 50 μm), and (I) the variations of pulmonary $CD11b^+$ BMDCs *vs.* CXCL12 level of lung tissue in pre-surgical (pre-) or post-surgical (post-) 4T1-tumor bearing mice ($n = 5$).

exact mass: 400.27) of TSPBA ($C_{21}H_{34}B_2Br_2N_2O_4$, exact mass: 558.11). Moreover, the structure and ROS-responsive lability of TSPBA were confirmed by ^{1}H NMR (Supporting Information Fig. S3). Finally, the syringeable solutions of (1) hydrogel precursor PVA and PDCs mixture and (2) crosslinker TSPBA and mAb mixture were mixed, and semi-solid hydrogel was immediately formed *via* the conjugation between the phenylboronic acid in TSPBA and the *cis*-1,3-diol in PVA. Because the fabricated hydrogel consisted of CXCR4-depleting PDC [P-$(LV)_6$], ICD-inducing PDCs (P-DOX) and PD-L1-blocking mAb, we termed such all-in-one drug depot as "hydrogel toolkit".

As shown in Fig. 2B, hydrogel precursor PVA without TSPBA crosslinking showed a typical rheology of solution, while storage modulus (G′) increased dramatically and exceeded loss modulus (G″) after the addition of TSPBA confirming the transformation into blank hydrogel. Meanwhile, hydrogel toolkit showed similar rheology properties with blank hydrogel, suggesting sol-to-gel formation was not affected by encapsulation of PDCs and mAb. In addition, cross-sectional scanning electron microscopy (SEM) images revealed a typical gel morphology with abundant porous structure for hydrogel toolkit (Fig. 2C). Furthermore, the confocal images of a frozen slice for hydrogel toolkit verified the PDCs and mAb were evenly distributed in the hydrogel matrix (Supporting Information Fig. S4).

Results in Fig. 2D showed that hydrogel toolkit displayed accelerated loss in volume when it was immersed in phosphate buffered saline (PBS, pH 7.4) containing 1 mmol/L H_2O_2, suggesting the ROS-sensitive degradation. Due to the selective breakdown of the hydrogel matrix, hydrogel toolkit exhibited ROS-responsive and sustained drug release (Fig. 2E). Within 3

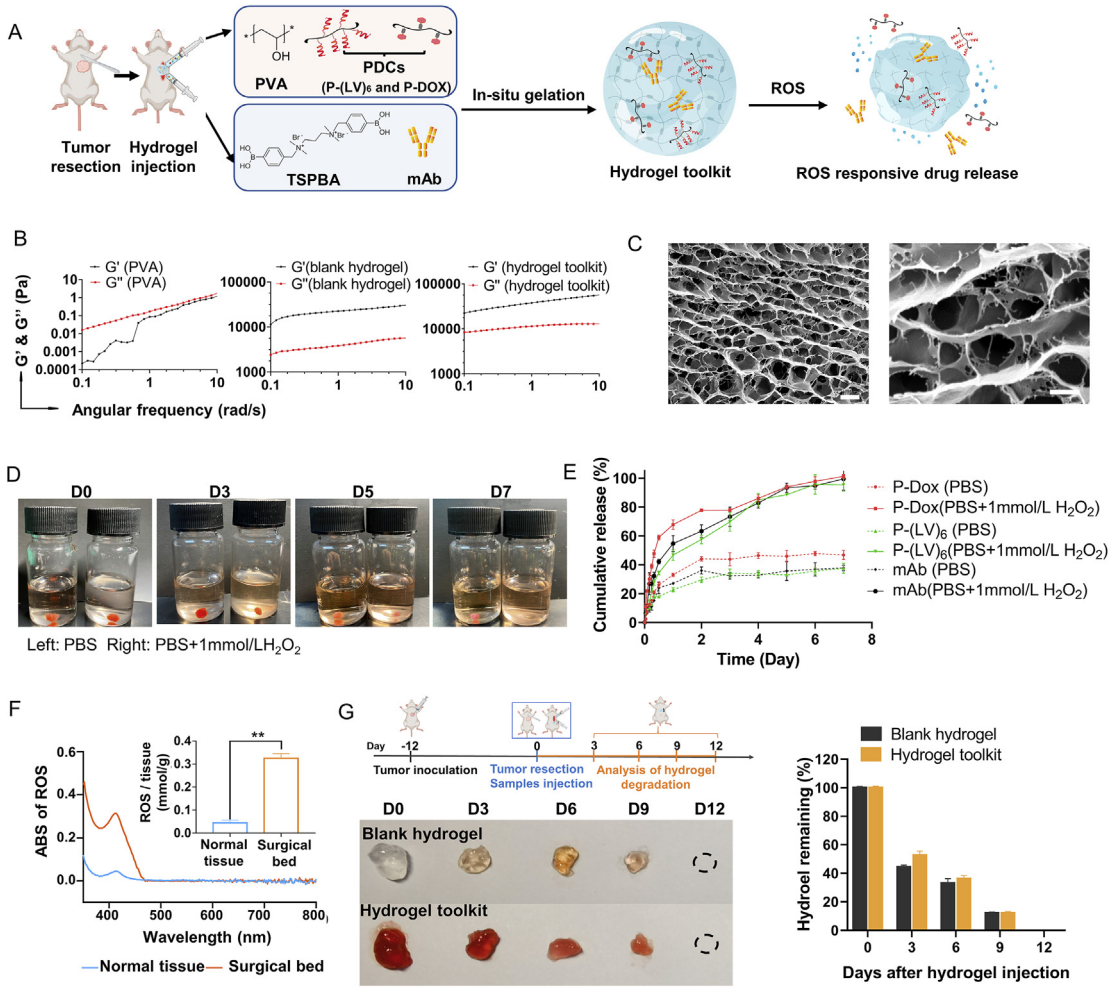

Figure 2 (A) Schematic illustration of a ROS-degradable gel scaffold loaded with PDCs and mAb (hydrogel toolkit). (B) Storage (G′) and loss (G″) modulus changes of the PVA, blank hydrogel and hydrogel toolkit. (C) SEM image of hydrogel toolkit. Left: scale bar = 2 μm. Right: zoom-in image of the scaffold, scale bar = 0.5 μm. (D) Morphology changes of hydrogel toolkit in PBS with and without H_2O_2 (1 mmol/L) over 7 days. (E) Cumulative release profiles of P-DOX, P-$(LV)_6$ and mAb from hydrogel toolkit incubated with PBS with or without H_2O_2 (1 mmol/L) (n = 3). (F) Changes of ROS level in the surgical bed after tumor resection. Data are presented as mean ± SD (n = 3); $^{**}P < 0.01$ *vs.* normal tissue group. (G) Representative optical images and the weight changes of blank hydrogel and hydrogel toolkit from the surgical bed after tumor resection for different time (n = 3). D: day.

days, approximately 80% of PDCs [P-$(LV)_6$ and P-Dox] and mAb were released in the presence of 1 mmol/L H_2O_2 while the extent of release was only 40% in PBS (pH 7.4) without 1 mmol/L H_2O_2. To further demonstrate the stimuli-responsive degradation of hydrogel toolkit in surgical trauma, we investigated whether the surgery would lead to enhanced ROS level. As shown in Fig. 2F, compared with normal tissue, tissue collected in the surgical sites showed markedly elevated ROS concentration. As a result, hydrogel toolkit displaced in the tumor resection cavity gradually degraded with decreased volume and weight, and completely disappeared on Day 12 after injection (Fig. 2G).

3.3. Hydrogel toolkit suppresses tumor recurrence and metastasis

An orthotopic breast tumor recurrence model undergoing an incomplete tumor resection was established to assess the therapeutic efficacy of hydrogel toolkit. BALB/c mice were inoculated with 4T1 breast cancer cells on Day 0, and surgery was performed with approximately 5% tumor tissue left intentionally on Day 12. Immediately afterward, blank hydrogel or hydrogel loaded with PDCs (PDCs@hydrogel), mAb (mAb@hydrogel) or their combination (hydrogel toolkit) was injected into the tumor resection cavity (Fig. 3A). As shown in Fig. 3B, postsurgical mice that were left untreated (control group) experienced rapid tumor regrowth, and blank hydrogel exerted minimal impact on inhibiting tumor recurrence. The effect of mAb@hydrogel, the PD-L1-blocking immunotherapy, was also limited, probably due to the increasingly immunosuppressive microenvironment of recurrent tumors. By comparison, PDCs@hydrogel, the CXCR4-depleting/ICD-inducing chemoimmunotherapy that was designed to reverse CXCR4-associated immunosuppression and increase ICD-associated immunogenicity, significantly slowed down the growth rate of recurrent tumors. Strikingly, hydrogel toolkit combining PDCs and mAb resulted in a further suppression on tumor regrowth showing 100% tumor inhibition and even 40% complete eradication, with a residual tumor volume and weight much smaller than any other groups (Fig. 3C and D).

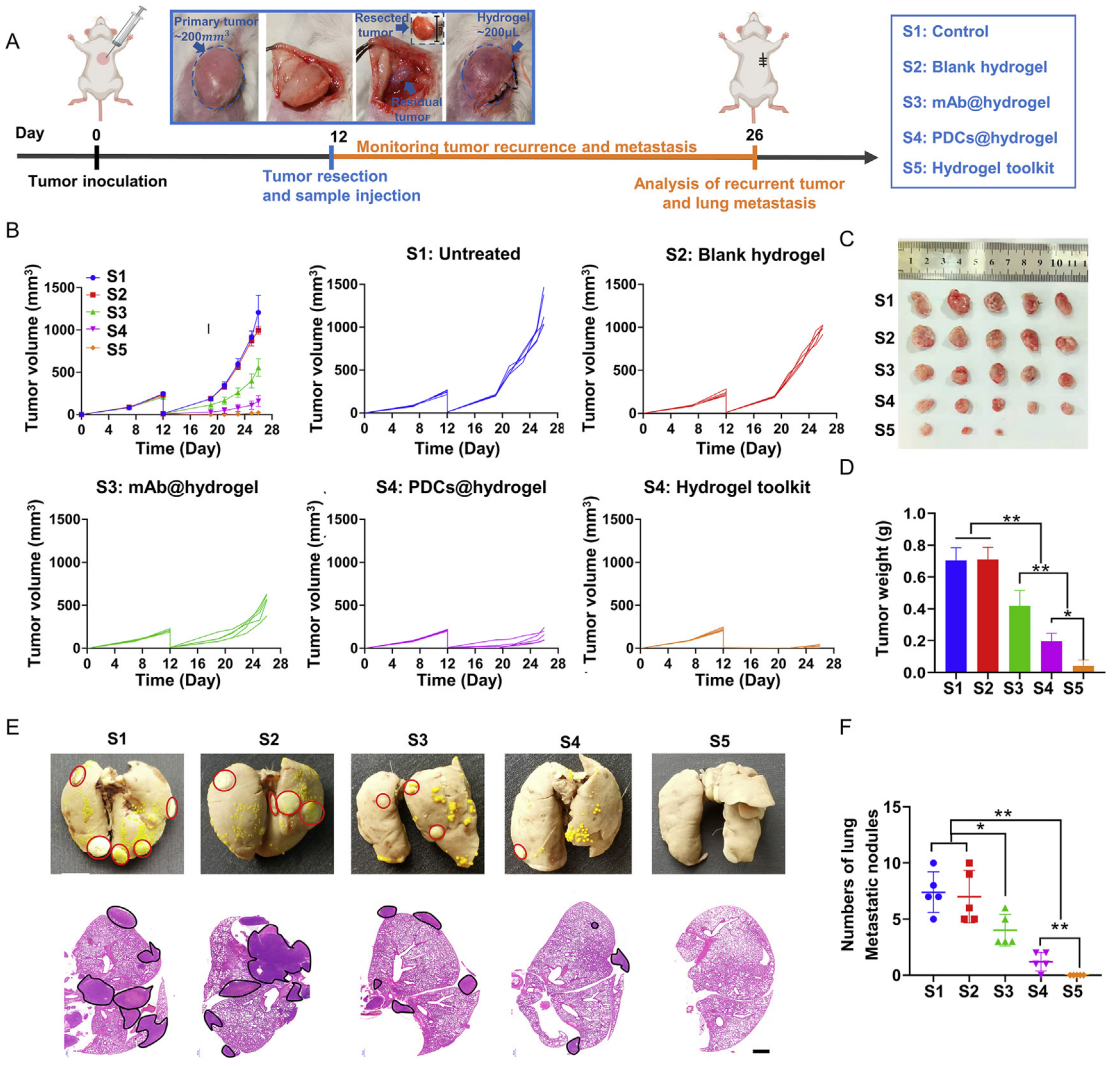

Figure 3 (A) Schematic illustration of treatment schedule. (B) Tumor growth curves, (C) images and (D) weight of recurrent tumors, (E) H&E histology analysis of lung lobe sections, and (F) numbers of pulmonary metastatic nodules in mice after 2-week postoperative period as indicated in (A) (scale bar = 500 μm). Data are presented as mean ± SD ($n = 5$); *$P < 0.05$ and **$P < 0.01$ *vs.* indicated.

Meanwhile, metastatic nodules of lungs harvested two weeks post operation were counted and visualized by H&E histology staining (Fig. 3E and F). As compared with mice in control and blank hydrogel groups that had obvious establishment of lung metastasis, PDCs@hydrogel and mAb@hydrogel-mitigated metastasis formation in lung, but to a limited extent. Markedly, no visible metastatic nodule was found in mice treated with hydrogel toolkit, suggesting complete prevention of postsurgical pulmonary metastasis.

To demonstrate the importance of ROS-responsiveness of hydrogel toolkit for local drug release, we generated ROS-unresponsive hydrogel toolkit as control (Supporting Information Fig. S5). Due to the absence of ROS-sensitive linker, unresponsive hydrogel showed similarly slow volume change and drug release rate in PBS with and without 1 mmol/L H_2O_2 (Fig. S5A and S5B). In addition, majority of unresponsive blank or drug-loaded hydrogel remained in the tumor resection cavity over 12 days (Fig. S5C). Consequently, despite loading with both PDCs and mAb, the ROS-unresponsive hydrogel toolkit only exerted moderate therapeutic efficacy to inhibit recurrent and metastatic tumors after surgery (Fig. S5D–S5F). By comparison, ROS-responsive hydrogel toolkit again showed prominent anti-tumor and anti-metastasis effect, highlighting the advantage of stimuli-responsive degradation and drug release for postsurgical application of hydrogel drug depot.

Moreover, no body weight loss, cardiotoxicity, or liver and kidney injuries were observed during the treatment (Supporting Information Fig. S6), demonstrating the biosafety. Collectively, these results validated that the hydrogel toolkit, an all-in-one local drug depot involving CXCR4 depletion, ICD induction, and PD-L1 inhibition, was an effective and safe postoperative prevention platform for tumor recurrence and metastasis.

3.4. Hydrogel toolkit remodels immune microenvironment of postsurgical residual tumor

Then we investigated the pharmacokinetics and biodistribution of Cy5-labled PDCs and mAb that were either loaded within locally administered hydrogel at surgical site or intravenously injected (Supporting Information Fig. S7). During a 12-day experiment

after a single dose, PDCs and mAb encapsulated in local hydrogel remained almost undetectable in blood circulation as compared with their counterparts that were directly injected into blood (Fig. S7A). This result suggested that PDCs and mAb barely leaked into vasculature after released from hydrogels. Further analysis of biodistribution revealed that PDCs and mAb within hydrogels could retain at surgical site for a long time, whereas intravenously administered samples insufficiently reached the postsurgical tumors (Fig. S7B). At the endpoint, PDCs and mAb within hydrogels primarily accumulated in tumor tissues and barely localized at other organs including the lung. In contrast, intravenously injected PDCs and mAb had relatively high level of distribution in liver and kidney (Fig. S7C and S7D). These results indicated local hydrogel depot for PDCs and mAb increased the contact with residual tumors and may potentially decrease the off-target toxicity.

The underlying mechanism of effective postsurgical treatment for hydrogel toolkit was further explored according to the schedule in Fig. 4A. Having confirmed surgery led to an immunosuppressive tumor microenvironment (Fig. 1), we first investigated whether the hydrogel toolkit could reverse the unfavorable alternation and prime anti-tumor immunity. Tumors were collected and analyzed at the endpoint of 2-week perioperative monitoring after treatment. Because of the involved functions of P-$(LV)_6$ and P-DOX, PDCs@hydrogel not only downregulated the expression of CXCR4 on tumor cells (Fig. 4B and Supporting Information Fig. S8), but also increased the intratumoral exposure of calreticulin (CRT), one of major hallmarks for ICD induction[26,27] (Fig. 4C and Fig. S8). Despite the ability to render tumor immunogenic, adaptive enrichment of PD-L1 was also observed in PDCs@hydrogel treatment due to a negative feedback response[28] (Fig. 4D and Fig. S8), which may explain the incomplete eradiation of tumor recurrence by PDCs@hydrogel. Meanwhile, although mAb@hydrogel efficiently reduced the population of PD-L1$^+$ tumor cells (Fig. 4D and Fig. S8), it failed to deplete CXCR4 or induce ICD (Fig. 4B, C and Fig. S8). In contrast, after packaging both PDCs and mAb in one hydrogel scaffold, hydrogel toolkit integrated the multifunction of ICD induction, CXCR4 depletion and PD-L1 blockade (Fig. 4B–D and Fig. S8).

As a result, hydrogel toolkit promoted dendritic cells (DCs) maturation with upregulated levels of costimulatory molecules including CD80 and CD86 (Suppporting Information Fig. S9), drastically reduced the frequencies of MDSCs (Fig. 4E) and Tregs (Fig. 4F), and considerably enhanced the tumor infiltration of CD8$^+$ T cells (Fig. 4F). Consistently, after treatment with hydrogel toolkit, the immunosuppressive cytokines, IL-10 and TGF-β, were significantly downregulated while the secretion of tumor reactive cytokine IFN-γ was upregulated (Fig. 4G). Together, these results suggested hydrogel toolkit was able to reprogram the postsurgical microenvironment of residual tumor to convert immunosuppressive tumor into immunostimulatory state.

3.5. *Hydrogel toolkit disrupts PMN formation in distant lung*

As mentioned above, the status of orthotopic tumor can be closely related to the formation of PMN in distant organ *via* a cascade of events: (1) initially, surgery stress stimulates the release of primary tumor-derived factors (*e.g.,* TGF-β and LOX) from resection cavity into blood circulation[22,23]; (2) these factors eventually accumulate at the pre-metastatic sites in lung and function as chemoattractant to facilitate the settlement of CD11b$^+$ BMDCs[29,30]; (3) then, CD11b$^+$ BMDCs increase vascular permeability by secreting MMP-9, induce immunosuppression by secreting IL-10, and further recruit more CD11b$^+$ BMDCs trafficking to lung by secreting S100A8 together creating pulmonary PMN[31–34]; (4) consequently, PMN releases chemoattractant such as CXCL12 to drive the metastasis of CXCR4$^+$ tumor cells, and provides fertile soil for the colony of disseminated tumor cell seeds[23,35–37]. Having demonstrated that hydrogel toolkit suppressed residual tumor by significantly shaping the microenvironment at the resection site, we next investigated its effect on influencing the pulmonary PMN to elucidate the complete eradication of postsurgical metastasis.

Two weeks after surgery, immunology analysis revealed significant establishment of PMN in lungs of untreated mice (control) as evidenced by drastically increased level of TGF-β and LOX in systemic circulation (Fig. 5A and B) and lung (Fig. 5C and D), enhanced pulmonary accumulation of CD11b$^+$BMDCs (Fig. 5E), and the PMN-fostering downstream of MMP-9, IL-10, S100A8 (Fig. 5F) as compared with that of tumor-free mice. Although mAb@hydrogel and PDCs@hydrogel separately attenuated these PMN parameters to some degrees, they failed to normalize the lung to a normal state. Thus, the effect of PMN still existed, which may explain that neither mAb@hydrogel or PDCs@hydrogel prevented the postsurgical metastasis (Fig. 3E and F).

Notably, local administration of hydrogel toolkit at surgical site profoundly disrupted the formation of PMN in distant lung, which could be ascribed to the prominent inhibition or even eradication of residual tumors. This was because that the tumor inhibition abrogated the release of primary tumor-secreted factors (*e.g.*, TGF-β and LOX) into blood circulation (Fig. 5A and B) and their accumulation in distant lung (Fig. 5C and D). Therefore, pulmonary recruitment of CD11b$^+$ BMDCs (Fig. 5E) and downstream of PMN-promoting pathways including MMP-9, IL-10, S100A8 (Fig. 5F) in hydrogel toolkit-treated mice were comparable with that of tumor-free mice. It was worth noting that the hydrogel toolkit-mediated PMN depletion was unlikely due to the direct effect from loaded drugs, because PDCs and mAb released from local hydrogel depot barely diffused into blood circulation and did not target distant lung (Fig. S7). Meanwhile, the pulmonary infiltration of CD8$^+$ T cells and Tregs were also regulated to achieve immune normalization in lungs of hydrogel toolkit-treated mice (Supporting Information Fig. S10).

As a result of disrupted PMN, hydrogel toolkit elicited greater inhibition of CXCL12 secretion in lung than other treatments (Fig. 5G). Combining with the results in Fig. 4, this meant that hydrogel toolkit-mediated interference of postsurgical CXCR4–CXCL12 axis upregulation involved two-pronged pathway: (1) inhibition of CXCR4 in residual tumor seeds and (2) inhibition of CXCL12 in distant PMN soil, together leading to the complete prevention of postsurgical metastasis as observed in Fig. 3.

3.6. *Hydrogel toolkit results in a long-term immune memory effect against postoperative tumor recurrence and metastasis*

We next investigated whether a single dose of hydrogel toolkit could induce a long-term memory against postsurgical tumor recurrence and metastasis. *In vivo* therapeutic study up to 100 days was performed with tumor inoculation (s.c.) on Day 0, surgical resection on Day 12, secondary tumor rechallenges (i.v.) of completely cured mice on Day 72, followed by three-weak observation until immune analysis at the endpoint (Fig. 6A). Results in Fig. 6B showed that all the mice in untreated control and blank hydrogel groups underwent tumor recurrence within 7 days

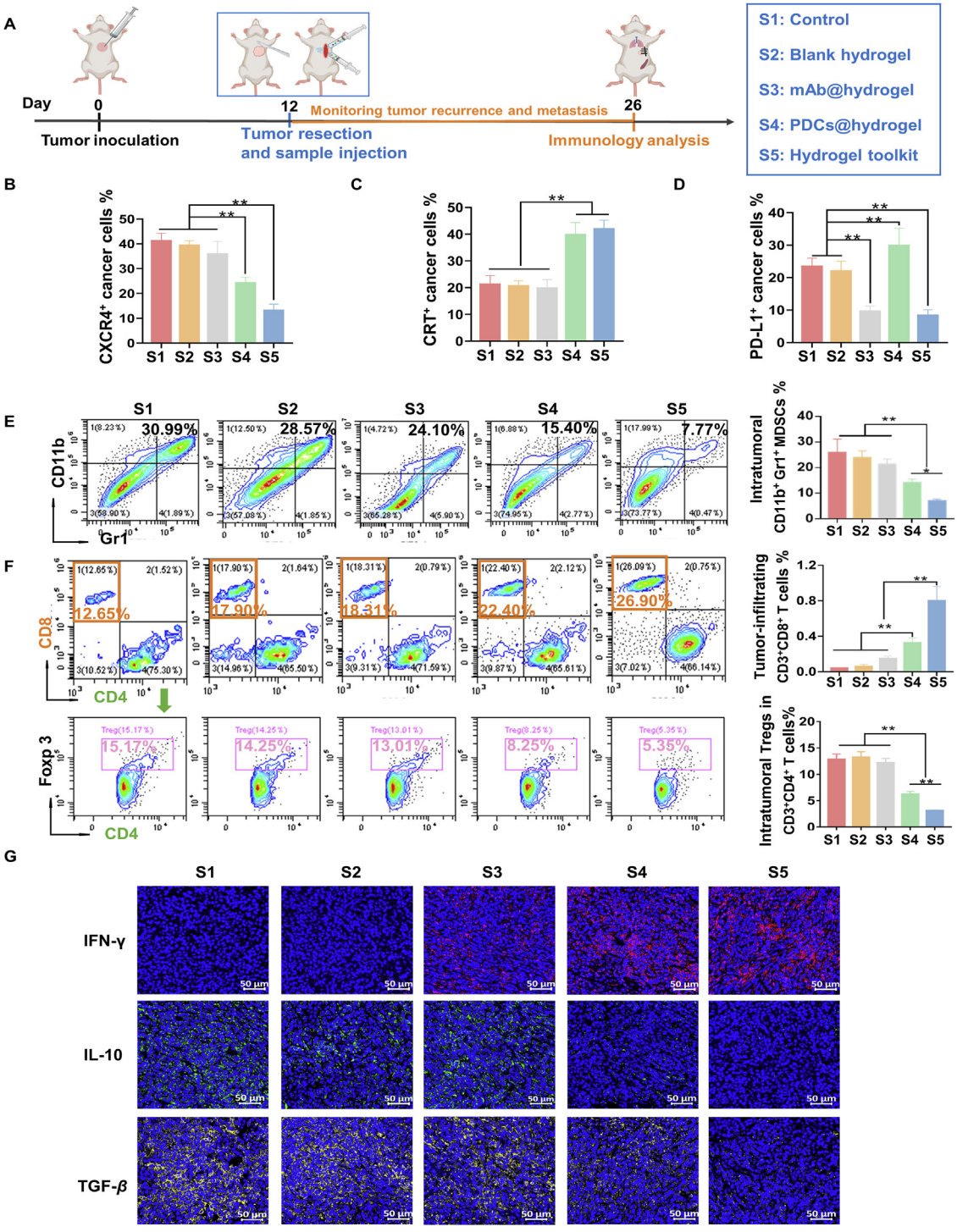

Figure 4 (A) Treatment schedule for immunology analysis. (B) The frequency of $CXCR4^+$ cancer cells, (C) tumor cells undergoing ICD (surface CRT^+ cells), (D) PD-$L1^+$ cancer cells, (E) intratumoral MDSCs ($CD11b^+Gr1^+$), (F) tumor-infiltrating $CD3^+CD8^+$ T cells and intratumoral Tregs ($CD3^+CD4^+Foxp3^+$), (G) intratumoral expression of IFN-γ, IL-10 and TGF-β in mice after treatments as indicated in (A) (scale bar = 50 μm). Data are presented as mean ± SD ($n = 5$); *$P < 0.05$ and **$P < 0.01$ *vs.* indicated.

and died rapidly within 23 days after tumor resection. Monotherapy of mAb@hydrogel or PDCs@hydrogel also showed a disappointing efficacy with 100% tumor recurrent rate within 30 days, and only prolonged the survival of mice to a limited extent. Notably, postsurgical treatment with hydrogel toolkit significantly extended the survival time, and 5 out of 10 mice underwent completely tumor eradication without further recurrence for two months after surgery. Moreover, even after a secondary tumor rechallenge, those cured mice achieved a 100% survival rate until the endpoint of whole experiment.

During the rechallenge analysis, bioluminescence imaging method was used to monitor the progression of intravenously injected 4T1-Luc breast cancer cells (Fig. 6C). Naïve mice and 4T1 tumor-bearing mice with subsequent tumor resection were also

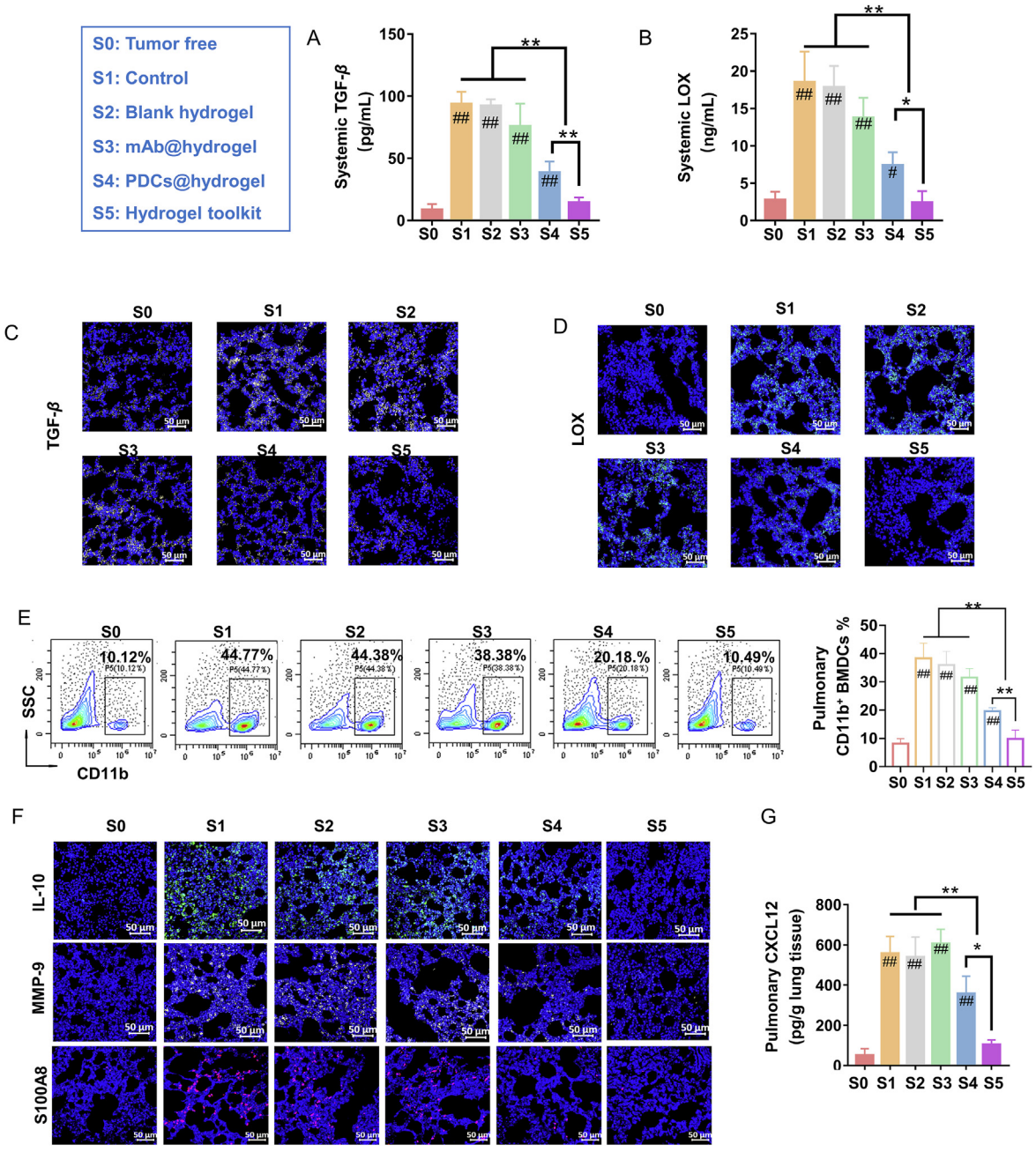

Figure 5 (A) TGF-β and (B) LOX level in serum, (C) pulmonary TGF-β and (D) LOX accumulation, (E) pulmonary CD11b$^+$BMDCs, (F) pulmonary IL-10, MMP-9, S100A8 expression and (G) pulmonary CXCL12 in mice after treatments as indicated in Fig. 4A (scale bar = 50 μm). Data are presented as mean ± SD ($n = 5$), $^*P < 0.05$, $^{**}P < 0.01$, $^{\#}P < 0.05$ and $^{\#\#}P < 0.01$ *vs.* tumor free group or indicated.

intravenously injected with 4T1-Luc cells to function as controls. The schedule for each group was also presented in Fig. 6C. Obvious lung metastasis (100% metastasis rate) was observed in naïve mice within one week. As compared to naïve mice, mice undergoing tumor resection showed systemic bioluminescence over the whole body and high mortality, probably due to the negative stimulation of surgery stress. In contrast, all the cured mice from the therapy of hydrogel toolkit were resistant to tumor rechallenge with a 100% survival rate for extra three weeks and no visible metastatic bioluminescence in 4/5 rechallenged mice. This suggested that post-surgical PMN with pro-metastasis function was disrupted by the hydrogel toolkit treatment. In addition, postsurgical intervention with hydrogel toolkit resulted in a significant higher frequency of memory effector CD8$^+$ T cells (CD44$^+$CD62L$^-$) in spleen than naïve or surgery control (Fig. 6D), suggesting the establishment of durable immunity against post-operative tumor recurrence and metastasis.

3.7. *Local administration of hydrogel toolkit exerts once-for-all effect by increasing therapeutic efficacy and decreasing off-target toxicity*

Previously, we reported the intravenous injection (i.v.) of PDC combination of P-DOX and P-(LV)$_6$ potentiated intraperitoneally administered (i.p.) anti-PD-L1 mAb to treat breast cancer[12]. Due to the adequate blood perfusion, abnormal vasculature, and dysfunctional lymphatic drainage in solid tumor, PDCs could

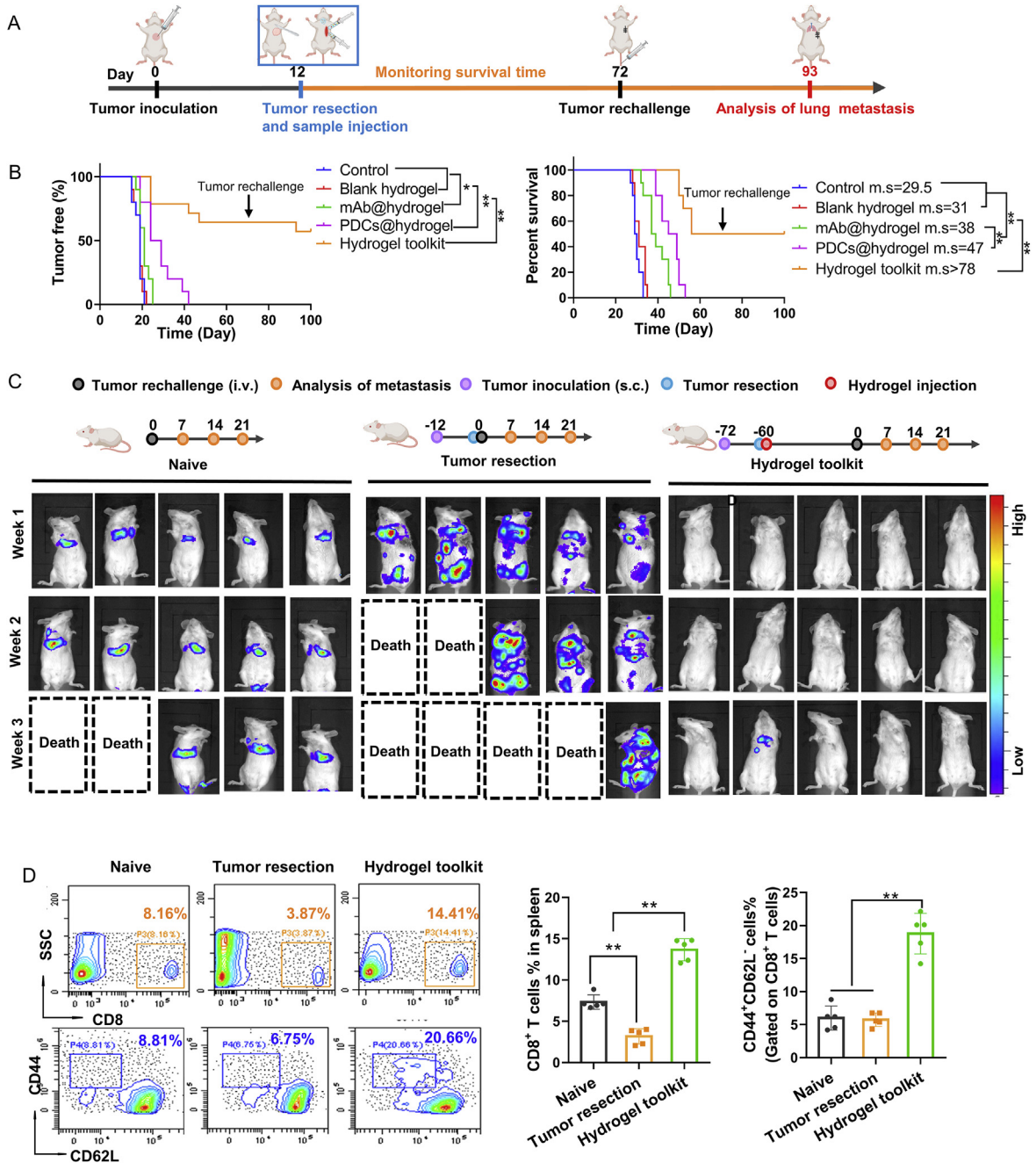

Figure 6 (A) Schematic illustration of treatment schedule and second tumor rechallenge. (B) The evolution of tumor recurrence and overall survival time of mice after tumor resection and different treatments. Survival curves were obtained using the Kaplan−Meier method and compared by the log-rank test. Data are presented as mean ± SD ($n = 10$); $^{*}P < 0.05$ and $^{**}P < 0.01$ *vs*. control group or indicated; m.s: median survival time. (C) Bioluminescence images of 4T1-Luc cells in mice, and (D) the frequency of $CD44^{+}CD62L^{-}$ memory effector $CD8^{+}$ T cells in the spleen at the endpoint after 4T1-Luc cells rechallenge. Data are presented as mean ± SD ($n = 5$); $^{**}P < 0.01$ *vs.* control or indicated.

passively accumulate in tumor where P-DOX induced ICD to recruit T cells and P-$(LV)_6$ depleted CXCR4 to revive T cells, together priming immunosuppressive tumors for PD-L1 blockade therapy. Since current study revealed that activation of CXCR4–CXCL12 axis at both residual tumor and pre-existing PMN exacerbated the immunosuppression of postsurgical cancer, the triple combination of CXCR4 inhibition, ICD induction and PD-L1 blockade strategies may hold great promise to interfere tumor recurrence and metastasis. However, the drug delivery method in previous study may not be applicable to postsurgical intervention, for the following two reasons: (1) residual tumors after surgery are tiny, scattered sporadically in the normal tissue of surgical incision, lacking typical features of tumor for targeting, and therefore may not be efficiently reached by PDCs *via* i.v. administration; (2) previous regimen requires i.v. injection of PDCs and i.p. injection of mAb every other day for four cycles to ensure desired intratumoral concentration, which can cause off-targeted toxicity and impair compliance of postoperative patients. Such dilemma emphasized the need for a once-for-all approach.

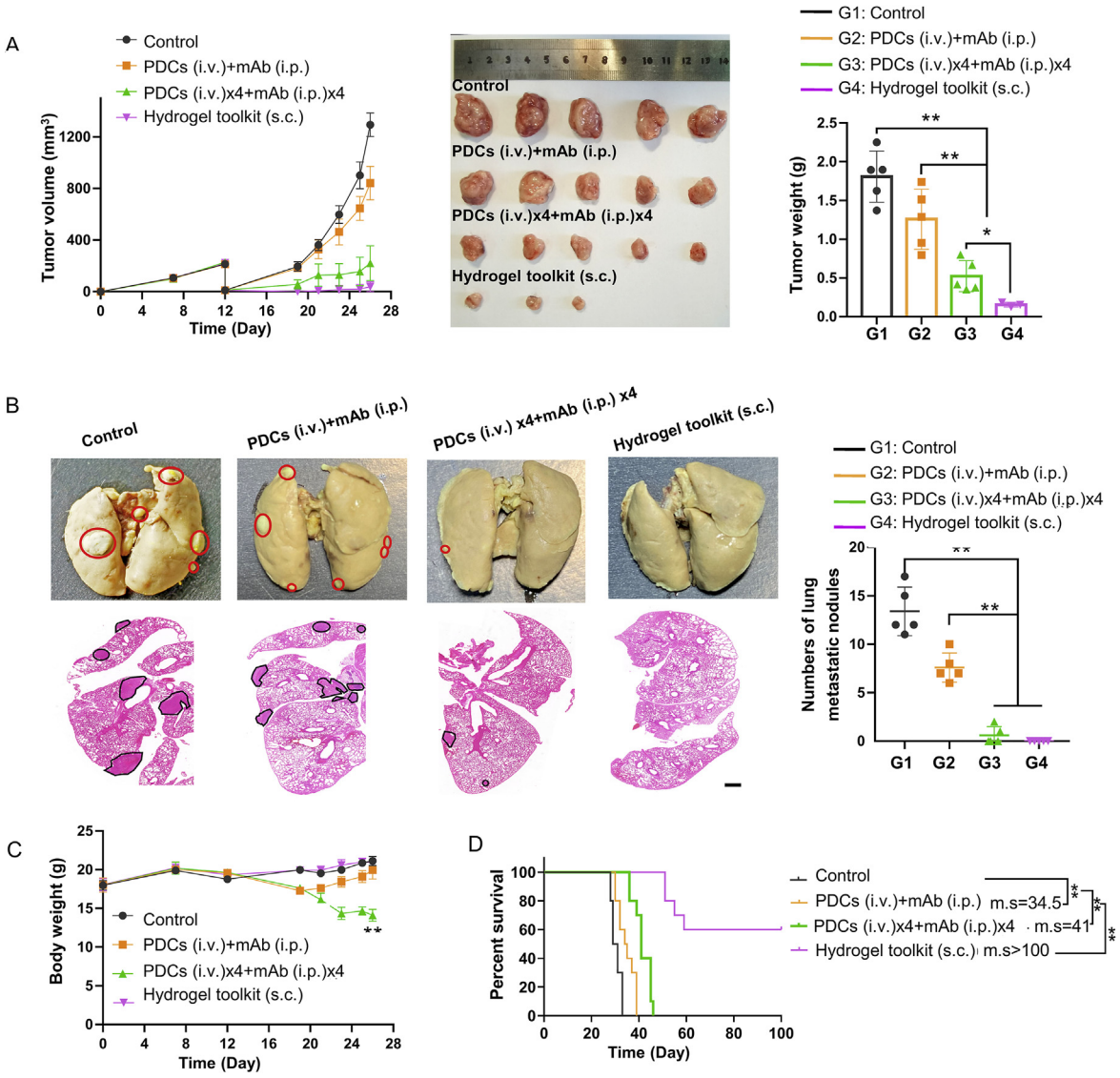

Figure 7 (A) Tumor growth curves over time during 2-week postoperative period, images of excised tumor and recurrent tumor weight at the endpoint of 2-week postoperative period. Data are presented as mean ± SD ($n = 5$); $^{*}P < 0.05$ and $^{**}P < 0.01$ *vs.* control group or indicated. (B) Metastatic nodules in lung at the endpoint of 2-week postoperative period (scale bar = 500 μm). Data are presented as mean ± SD ($n = 5$); $^{**}P < 0.01$ *vs.* indicated. (C) Body weight of mice over time during 2-week postoperative period. Data are presented as mean ± SD ($n = 5$); $^{**}P < 0.01$ *vs.* indicated. (D) Overall survival time of mice after tumor resection and different treatments. Survival curves were obtained using the Kaplan−Meier method and compared by the log-rank test. Data are presented as mean ± SD ($n = 10$); $^{**}P < 0.01$ *vs.* control group or indicated; m.s: median survival time.

To this end, an all-in-one hydrogel toolkit loaded with PDCs and mAb was designed, for the purposes that (1) *in situ* formation of hydrogel toolkit after subcutaneous (s.c.) injection of syringeable hydrogel precursor and crosslinker would fit the irregular surgical trauma and enable direct contact with residual microtumors at the edge of resection; (2) gradual degradation of hydrogel would enable sustained drug release for durable effect. To confirm the advantages of local administration of hydrogel toolkit, therapeutic efficacy of its single dose was investigated in another individual experiment and compared with single administration of PDCs (i.v.) + mAb (i.p.) and repeated administrations of PDCs (i.v.)×4 + mAb (i.p.)×4, noting that every single dose for each treatment is of the same drug equivalence (DOX, 5 mg/kg; LV, 1 mg/kg; mAb, 2.5 mg/kg). Results showed that postsurgical intervention with hydrogel toolkit generated reproducible effect to suppress the growth of residual tumor (Fig. 7A) and prevent the pulmonary metastasis (Fig. 7B), because of its local effect on inhibiting cancer cell "seeds" and abscopal effect on disturbing pre-metastatic "soil" as demonstrated above. By comparison, the therapeutic outcome of PDCs (i.v.) + mAb (i.p.) was unsatisfactory with moderate inhibition on tumor recurrence and metastasis. Further increasing the injection frequency to PDCs (i.v.)×4 + mAb (i.p.)×4 still showed less efficacy than single dosed hydrogel toolkit, but increased the toxicity as evidenced by the significant loss in body weight thereafter (Fig. 7C) and 100% mortality rate within 50 days (Fig. 7D). In contrast, weight loss was not observed in mice receiving local therapy of hydrogel toolkit, and their survival time was significantly extended. These results demonstrated that a single dose of hydrogel toolkit could serve as all-in-one drug depot for *in situ* delivery of PDCs and mAb to surgical site, and exert once-for-all effect for postsurgical intervention by increasing therapeutic efficacy and decreasing off-target toxicity.

4. Conclusions

In summary, an all-in-one and once-for-all hydrogel platform was developed for inhibition of postoperative tumor recurrence and metastasis. Immunology analysis revealed that postsurgical upregulation of CXCR4–CXCL12 axis at both residual tumor and pre-existing PMN exacerbated the immunosuppression and facilitated the metastasis. In this regard, an *in situ* formed hydrogel toolkit was designed in this study, which involved two PDCs to inhibit CXCR4–CXCL12 axis and increase tumor immunogenicity, respectively and one mAb to block adaptive upregulation of PD-L1. We demonstrated that such drug depot exerted both local effect on inhibiting residual tumor "seeds" at surgical trauma and abscopal effect on disturbing pre-existing PMN "soil" in distant lung. For local effect, injection of hydrogel toolkit at resection cavity enabled direct contact with residual microtumors and gradually released PDCs and mAb in response to elevated level of ROS in surgical trauma. As a result of CXCR4 inhibition, ICD induction, and PD-L1 blockade, anti-tumor immunity was provoked turning residual tumor seeds into an *in situ* vaccine. For abscopal effect, the influence from postsurgical tumor to promote pulmonary PMN formation was ceased, because hydrogel toolkit prominently alerted the secretion of cytokines (TGF-β, IL-10 and IFN-γ) in tumor microenvironment, and minimized the release of tumor-derived factors (TGF-β and LOX) to lung. This led to significant reduction of various PMN-fostering factors including the pulmonary BMDCs, IL-10, S100A8 and MMP-9. Consequently, abnormal PMN soil was repaired, and lung was normalized to a normal state. Furthermore, hydrogel toolkit could generate a long-term anti-tumor memory effect that was 100% resistant to a secondary tumor rechallenge. Importantly, *in situ* delivery of PDCs and mAbs to surgical site *via* hydrogel toolkit was able to eradicate recurrent tumors and completely prevent pulmonary metastasis with one single dose and less off-target toxicity.

Acknowledgment

The authors gratefully acknowledge financial support from National Natural Science Foundation of China (Grant Nos. 81625023 and 82104103).

Author contributions

Minglu Zhou designed the research, carried out the experiments, performed data analysis and wrote the manuscript. Qingting Zuo participated part of the experiments. Yuan Huang provided experimental resources and revised the manuscript. Lian Li supervised the work and revised the manuscript. All of the authors have read and approved the final manuscript.

Conflicts of interest

The authors declare no conflicts of interest.

Appendix A. Supporting information

Supporting data to this article can be found online at https://doi.org/10.1016/j.apsb.2022.02.017.

References

1. Demicheli R, Retsky MW, Hrushesky WJM, Baum M, Gukas ID. The effects of surgery on tumor growth: a century of investigations. *Ann Oncol* 2008;**19**:1821−8.
2. Hofer SO, Shrayer D, Reichner JS, Hoekstra HJ, Wanebo HJ. Wound-induced tumor progression: a probable role in recurrence after tumor resection. *Arch Surg* 1998;**133**:383−9.
3. Hamard L, Ratel D, Selek L, Berger F, Sanden BVD, Wion D. The brain tissue response to surgical injury and its possible contribution to glioma recurrence. *J Neuro Oncol* 2016;**128**:1−8.
4. Zhang YY, Wang TG, Tian Y, Zhang CN, Ge K, Zhang JC, et al. Gold nanorods-mediated efficient synergistic immunotherapy for detection and inhibition of postoperative tumor recurrence. *Acta Pharm Sin B* 2021;**11**:1978−92.
5. Mahoney KM, Rennert PD, Freeman GJ. Combination cancer immunotherapy and new immunomodulatory targets. *Nat Rev Drug Discov* 2015;**14**:561−84.
6. Couzin-Frankel J. Breakthrough of the year 2013. Cancer immunotherapy. *Science* 2013;**342**:1432−3.
7. Fan Q, Ma QL, Bai JY, Xu JL, Fei ZY, Dong ZL, et al. An implantable blood clot-based immune niche for enhanced cancer vaccination. *Sci Adv* 2020;**6**:eabb4639.
8. Predina J, Eruslanov E, Judy B, Kapoor V, Cheng GJ, Wang LC, et al. Changes in the local tumor microenvironment in recurrent cancers may explain the failure of vaccines after surgery. *Proc Natl Acad Sci U S A* 2013;**110**:E415−24.
9. Hu M, Zhang J, Yu YL, Tu K, Yang T, Wang Y, et al. Injectable liquid crystal formation system for reshaping tumor immunosuppressive microenvironment to boost antitumor immunity: postoperative chemoimmunotherapy. *Small* 2020;**16**:2004905.
10. Bosiljcic M, Cederberg RA, Hamilton MJ, LePard NE, Harbourne BT, Collier JL, et al. Targeting myeloid-derived suppressor cells in combination with primary mammary tumor resection reduces metastatic growth in the lungs. *Breast Cancer Res* 2019;**21**:1−16.
11. Lu ZH, Zou JL, Li S, Topper MJ, Tao Y, Zhang H, et al. Epigenetic therapy inhibits metastases by disrupting premetastatic niches. *Nature* 2020;**579**:284−90.
12. Zhou ML, Luo CH, Zhou Z, Li L, Huang Y. Improving anti-PD-L1 therapy in triple negative breast cancer by polymer-enhanced immunogenic cell death and CXCR4 blockade. *J Control Release* 2021;**334**:248−62.
13. Wang C, Wang JQ, Zhang XD, Yu SJ, Wen D, Hu QY, et al. *In situ* formed reactive oxygen species−responsive scaffold with gemcitabine and checkpoint inhibitor for combination therapy. *Sci Transl Med* 2018;**10**:eaan3682.
14. Bu LL, Yan JJ, Wang ZJ, Ruan HT, Chen Q, Gunadhi V, et al. Advances in drug delivery for post-surgical cancer treatment. *Biomaterials* 2019;**219**:119182.
15. Li XL, Xu FN, He Y, Li Y, Hou JW, Yang G, et al. A hierarchical structured ultrafine fiber device for preventing postoperative recurrence and metastasis of breast cancer. *Adv Funct Mater* 2020;**30**:2004851.
16. Wang JQ, Ye YQ, Yu JC, Kahkoska AR, Zhang XD, Wang C, et al. Core−shell microneedle gel for self-regulated insulin delivery. *ACS Nano* 2018;**12**:2466−73.
17. Zhang YQ, Wang JQ, Yu JC, Wen D, Kahkoska AR, Lu Y, et al. Bioresponsive microneedles with a sheath structure for H_2O_2 and pH cascade-triggered insulin delivery. *Small* 2018;**14**:1704181.
18. Ruan HT, Hu QY, Wen D, Chen Q, Chen GJ, Lu YF, et al. A dual-bioresponsive drug-delivery depot for combination of epigenetic modulation and immune checkpoint blockade. *Adv Mater* 2019;**31**:1806957.
19. Xu Y, Liu JW, Liu ZY, Ren H, Yong JH, Li WL, et al. Blockade of platelets using tumor-specific no-releasing nanoparticles prevents

tumor metastasis and reverses tumor immunosuppression. *ACS Nano* 2020;**14**:9780−95.
20. Hiller JG, Perry NJ, Poulogiannis G, Riedel B, Sloan EK. Perioperative events influence cancer recurrence risk after surgery. *Nat Rev Clin Oncol* 2018;**15**:205−18.
21. Zhao HJ, Song QL, Zheng CX, Zhao BB, Wu LX, Feng QH, et al. Implantable bioresponsive nanoarray enhances postsurgical immunotherapy by activating pyroptosis and remodeling tumor microenvironment. *Adv Funct Mater* 2020;**30**:2005747.
22. Cox TR, Rumney RMH, Schoof EM, Perryman L, Hoye AM. The hypoxic cancer secretome induces pre-metastatic bone lesions through lysyl oxidase. *Nature* 2015;**522**:106−10.
23. Zhou Y, Han M, Gao JQ. Prognosis and targeting of pre-metastatic niche. *J Control Release* 2020;**325**:223−34.
24. Wang YG, Ding YX, Guo NZ, Wang SJ. MDSCs: key criminals of tumor pre-metastatic niche formation. *Front Immunol* 2019;**10**:00172.
25. Teicher BA, Fricker SP. CXCL12 (SDF-1)/CXCR4 pathway in cancer. *Clin Cancer Res* 2010;**16**:2927−31.
26. Xiang YC, Chen LQ, Li L, Huang Y. Restoration and enhancement of immunogenic cell death of cisplatin by coadministration with digoxin and conjugation to hpma copolymer. *ACS Appl Mater Interfaces* 2019;**12**:1606−16.
27. Li W, Yang J, Luo LH, Jiang MS, Qin B, Yin H, et al. Targeting photodynamic and photothermal therapy to the endoplasmic reticulum enhances immunogenic cancer cell death. *Nat Commun* 2019;**10**:3349.
28. Li L, Li YC, Yang CH, Radford DC, Wang JW, Janát-Amsbury M, et al. Inhibition of immunosuppressive tumors by polymer-assisted inductions of immunogenic cell death and multivalent PD-L1 cross-linking. *Adv Funct Mater* 2020;**30**:1908961.
29. Erler JT, Bennewith KL, Cox TR, Lang G, Bird D, Koong A, et al. Hypoxia-induced lysyl oxidase is a critical mediator of bone marrow cell recruitment to form the premetastatic niche. *Cancer Cell* 2009;**15**:35−44.
30. Hiratsuka S, Watanabe A, Aburatani H, Maru Y. Tumour-mediated upregulation of chemoattractants and recruitment of myeloid cells predetermines lung metastasis. *Nat Cell Biol* 2006;**8**:1369−75.
31. Yan HH, Pickup M, Pang YL, Gorska AE, Li ZY, Chytil A, et al. Gr-1^{+}CD11b^{+} myeloid cells tip the balance of immune protection to tumor promotion in the premetastatic lung. *Cancer Res* 2010;**70**:6139−49.
32. Peinado H, Rafii S, Lyden D. Inflammation joins the "niche". *Cancer Cell* 2008;**14**:347−9.
33. Hiratsuka S, Goel S, Kamoun WS, Maru Y, Fukumura D, Duda DG, et al. Endothelial focal adhesion kinase mediates cancer cell homing to discrete regions of the lungs *via* E-selectin up-regulation. *Proc Natl Acad Sci U S A* 2011;**108**:3725−30.
34. Liu Y, Cao XT. Immunosuppressive cells in tumor immune escape and metastasis. *J Mol Med* 2016;**94**:509−22.
35. Mortezaee K. CXCL12/CXCR4 axis in the microenvironment of solid tumors: a critical mediator of metastasis. *Life Sci* 2020;**249**:117534.
36. Arya M, Ahmed H, Silhi N, Williamson M, Patel H. Clinical importance and therapeutic implications of the pivotal CXCL12-CXCR4 (chemokine ligand-receptor) interaction in cancer cell migration. *Tumor Biol* 2007;**28**:123−31.
37. Wu JY, Long Y, Li M, He Q. Emerging nanomedicine-based therapeutics for hematogenous metastatic cascade inhibition: interfering with the crosstalk between "seed and soil". *Acta Pharm Sin B* 2021;**11**:2286−305.